



Nanoscale

How Structural and Vibrational Features Affect Optoelectronic Properties of Non-Stoichiometric Quantum Dots: Computational Insights

Journal:	<i>Nanoscale</i>
Manuscript ID	NR-ART-12-2022-006785.R1
Article Type:	Paper
Date Submitted by the Author:	15-Mar-2023
Complete List of Authors:	Bhati, Manav; Rice University, Chemical Engineering Ivanov, Sergei; Los Alamos National Laboratory, Chemistry division Senftle, Thomas; Rice University, Tretiak, Sergei; Los Alamos National Laboratory, Theoretical Division Ghosh, Dibyajyoti; IIT Delhi,

SCHOLARONE™
Manuscripts

How Structural and Vibrational Features Affect Optoelectronic Properties of Non-Stoichiometric Quantum Dots: Computational Insights

Manav Bhati,^{a,b,c} Sergei A. Ivanov,^{d,e} Thomas P. Senftle,^c Sergei Tretiak,^{a,b,e,*}

Dibyajyoti Ghosh ^{a,b,e,f*}

^a *Theoretical Division, Los Alamos National Laboratory, Los Alamos, NM, 87545, USA*

^b *Center for Nonlinear Studies, Los Alamos National Laboratory, Los Alamos, NM, 87545, USA*

^c *Department of Chemical and Biomolecular Engineering, Rice University, 6100 Main Street, Houston, TX 77005-1892, USA*

^d *Materials Physics and Applications Division, Los Alamos National Laboratory, Los Alamos, New Mexico, 87545 USA*

^e *Center for Integrated Nanotechnologies, Los Alamos National Laboratory, Los Alamos, NM, 87545, USA*

^f *Department of Materials Science and Engineering and Department of Chemistry, Indian Institute of Technology, Delhi, Hauz Khas, New Delhi 110016, India*

* Corresponding authors; E-mails: serg@lanl.gov, dibyajyoti@iitd.ac.in

Abstract

While stoichiometric quantum dots (QDs) have been well studied, a significant knowledge gap remains in the atomistic understanding of the non-stoichiometric ones, which are predominantly present during the experimental synthesis. Here, we investigate the effect of thermal fluctuations on structural and vibrational properties of non-stoichiometric cadmium selenide (CdSe) nanoclusters: anion-rich (Se-rich) and cation-rich (Cd-rich) using *ab-initio* molecular dynamics (AIMD) simulations. While the excess atoms on the surface fluctuate more for a given QD type, the optical phonon modes are mostly composed of Se atoms dynamics, irrespective of the composition. Moreover, Se-rich QDs have higher bandgap fluctuations compared to Cd-rich QDs, suggesting poor optical properties of Se-rich QDs. Additionally, non-adiabatic molecular dynamics (NAMD) suggests faster non-radiative recombination for Cd-rich QDs. Altogether, this work provides insights into the dynamic electronic properties of non-stoichiometric QDs and proposes a rationale for the observed optical stability and superiority of cation-rich candidates for light emission applications.

Colloidal QDs of II-VI and III-V materials are semiconductor nanocrystals synthesized in solution, whose small size gives rise to significant quantum confinement effects^{1,2} and size-dependent optoelectronic properties.³ Because of their tunable properties, these materials have attracted several applications.⁴⁻¹¹ Most of these applications require QDs that are uniform in size and composition. However, solution-based synthesis of QDs, although facile and economical, does not yield complete uniformity in size and composition distributions.¹² As a result, colloidal nanocrystals typically lack an exact stoichiometric 1:1 ratio of cations and anions in their structures - such QDs are referred to as “non-stoichiometric”. The imbalance in the net charge of the non-stoichiometric QDs is compensated by charge-neutralizing ligands that coordinate with atoms on the surface. It is important to emphasize that the non-stoichiometry in these materials is not always undesirable and is particularly beneficial for photocatalytic applications.¹³⁻¹⁵ The importance of non-stoichiometric QDs and their ubiquitous presence in experiments are yet to be met with the respective theoretical modeling at the atomic scale.

Atomistic simulations can provide insights into phenomena associated with surface defects that are often difficult to study experimentally.¹⁶ Since the early works of *ab initio* calculations on CdSe QD,^{17,18} several computational studies have proved to be pivotal in understanding the photophysics of QDs, including studies on the effects of surfaces, passivating ligands, and dielectric solvent media on optoelectronic properties.¹⁹⁻²⁹ Most of these studies have been performed on magic-size QD clusters, which are small in size and thus are in the realm of computations. Such clusters are far from the common experimental QDs in terms of size and properties because of their high fraction of surface and ligand atoms. Yet, they are considered suitable to act as a bridge between theory and experiments as such small clusters can be synthesized experimentally.³⁰ These magic-size clusters are therefore considered valuable to gain insights into the atomic scale phenomena using computational simulations. Notably, these magic-size clusters do not represent the diversity of QD clusters. They represent only a small part of possible QD structures that are stoichiometric. Non-stoichiometric QDs are practically inevitable in solution-based experimental synthesis and remain largely unrepresented in most of the theoretical studies.³¹ We attempted to bridge the existing knowledge gap by investigating the optical and electronic properties of non-stoichiometric CdSe QDs in our previous article³² and have focused on understanding the thermal effects on optoelectronics properties in this work. Our choice of QDs in these studies has been reasonable as we have employed small QD clusters that are non-

stoichiometric and have a size comparable to magic-size clusters (~ 1.5 nm in diameter), making them computationally feasible. Moreover, similar systems have been synthesized experimentally. Therefore, we believe that our QD clusters can act as bridges between experiments and theory, similar to magic-size clusters but for non-stoichiometric QDs.

In our previous work, we employed time-dependent density functional theory (TDDFT) to understand how electronic excitations are affected by the stoichiometry of the QDs. All of our previous simulations were carried out for the ground state static structures of QDs optimized at 0 K. However, it is also important to understand the dynamic behavior of these materials and how their properties evolve due to thermal effects at ambient conditions. It has been emphasized that these thermal fluctuations affect the structures of nanosized crystals significantly, thereby influencing optoelectronic properties.^{33–35} In our recent work,³³ we applied AIMD simulations to investigate the effects of thermal fluctuations on the properties of stoichiometric $\text{Cd}_{33}\text{Se}_{33}$. We found that the surface atoms are more dynamic than the core atoms and their dynamics greatly influence the photophysics of QDs. Several other computational and experimental studies have provided conclusive evidence for the influence of surface fluctuations and modifications on the photophysical properties of QDs,^{36–39} where surface-associated fluctuations in electronic structure would broaden the emission spectra, thereby diminishing the potential application of QDs in single-photon emitters⁴⁰ (SPEs). Therefore, it is of utmost importance to investigate the influence of thermal fluctuations on the optoelectronic properties of non-stoichiometric QDs and understand the role of their surface atoms. Here, we aim to obtain such insights by investigating both Se-rich and Cd-rich QDs of similar sizes (~ 15 Å in diameter) using long AIMD trajectories (~ 35 ps) at 300 K to understand the evolution of their structural, vibrational, and optoelectronic properties.

Structural Dynamics

The initial structure of Se-rich QD is based on the $\text{Cd}_{17}\text{Se}_{28}$ cluster, previously characterized experimentally,^{41,42} and the initial structure of Cd-rich QD is obtained by switching Se/Cd atom placement in Se-rich QD. The Se-rich and Cd-rich QDs have excess Se^{2-} anions and Cd^{2+} cations, respectively. Overall, the structures are made charge-neutral via the coordination of charge-neutralizing ligands on the surface: H^+ for Se-rich ($\text{Cd}_{17}\text{Se}_{28}\text{H}_{22}$) and Cl^- for Cd-rich ($\text{Cd}_{28}\text{Se}_{17}\text{Cl}_{22}$). Other than neutralizing the QDs, these ligands also serve as a good approximation for experimentally used ligands by enabling us to model dynamics using AIMD simulations at

picosecond timescales. First, the ground state structures (derived from our previous work)³² are heated from 0 K to 300 K and equilibrated. Then, the structures are further evolved at 300 K in a microcanonical NVE ensemble for 35 ps. Trajectories from the final 10 ps of the simulation are utilized for the analysis of various properties. We note that these AIMD simulations were performed in the gas-phase environment. In our previous work,³² we found that the polarization continuum model for non-periodic QD systems stabilized the electronic states of surface atoms. However, in the current work, our focus is on understanding the differences in QDs due to thermal effects, where the effect of solvation might be insignificant or equivalent to the QDs considered. Further details are provided in the Supplemental Materials.

The resulting structures of Se-rich and Cd-rich QDs after 35 ps of AIMD simulations are shown in **Figure 1a**. The dynamical structures of QDs are characterized by the root-mean-square fluctuations (RMSF), which provide an estimate of the thermally influenced mobility of atomic sites. **Figure 1b** presents the calculated RMSF of both Se-rich and Cd-rich QDs. We find that Se atoms have higher fluctuations compared to Cd atoms in Se-rich QD, whereas Cd atoms have higher fluctuations compared to Se atoms in Cd-rich QD. For the QDs considered in this work, two surface atoms are not bonded to ligands as a result of charge neutrality. This makes several ligand arrangements possible on the QD surface in the realistic system and to capture this, we perform similar AIMD simulations on five additional QD configurations for each QD type, consistent with our previous work.³² These five QD configurations have the same atomic arrangement of Cd and Se within the cluster but have different arrangements of ligands on the surface. More details of these structural configurations are provided in our previous work³² and **Figure S1** in the Supplemental Information. We find that all these configurations have a consistent trend of RMSF, with Se atoms fluctuating more in Se-rich and Cd atoms fluctuating more in Cd-rich QDs (**Figure S2**). Usually, lighter atoms have higher fluctuations, but here, we find that the atomic mass is a less important factor compared to the atomic placement (in the core or on the surface) in determining the structural fluctuations. The surface atoms in these QDs are in a low-coordination environment having more spatial degrees of freedom compared to the coordinatively-saturated core atoms. Therefore, the surface atoms fluctuate more than the core atoms. These results are in complete agreement with the analysis of structural dynamics of stoichiometric QDs,³³ suggesting that this is a general phenomenon that is independent of QD stoichiometric ratio. As

we show below, the surface dynamics in conjunction with the non-stoichiometric composition of QDs leads to bewildering but pronounced effects on their optoelectronic properties.

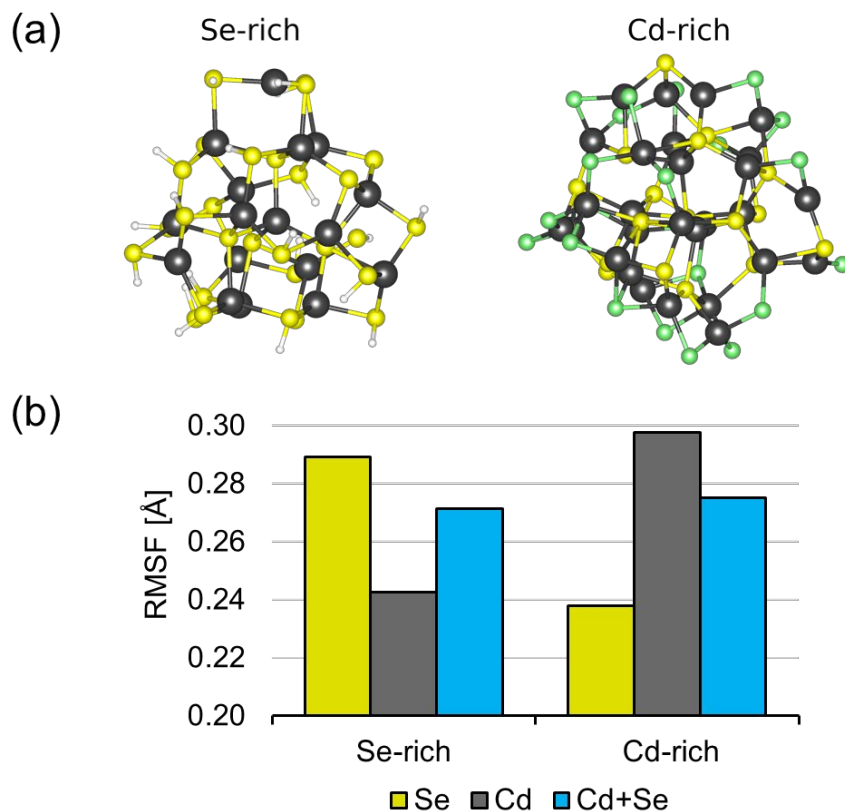


Figure 1. (a) Atomic structures of Se-rich and Cd-rich QDs after 35 ps of AIMD simulation at 300 K. Atoms in yellow: Se, grey: Cd, white: H, green: Cl. (b) The root-mean-square fluctuation (RMSF) of Se, Cd and Cd+Se atoms in Se-rich and Cd-rich QDs from the last 10 ps of the simulation.

Vibrational Dynamics

From the AIMD trajectories, the Fourier transform of the velocity autocorrelation function of atoms in the QD is calculated to determine the vibrational power spectra (**Figure 2a**). There are two important regions in these power spectra: low-frequency region ($< 120 \text{ cm}^{-1}$), and high-frequency region ($> 120 \text{ cm}^{-1}$). The low-frequency region is associated with prototypical acoustic phonon modes, which involve concerted motions of atoms around their equilibrium positions. The high-frequency region corresponds to prototypical optical modes, which involve an out-of-phase movement of atoms.^{33,43} These modes are typically activated by optical excitations and feature strong electron-phonon coupling, which ultimately influences the optoelectronic properties of the

material.^{44–46} The low-frequency acoustic modes also influence the electronic properties, such as pure dephasing, which would be discussed later. In **Figure 2a**, we have decomposed the overall spectra (black) into the contributions originating from Se and Cd atoms. The acoustic region ($< 120 \text{ cm}^{-1}$) is mainly dominated by the surface atoms (Se and Cd atoms contribute more to these motions in Se-rich and Cd-rich QDs, respectively). However, the nature of optical phonon modes is different, as they are predominantly bond vibrations associated with the motions of light Se atoms, irrespective of the type of QD. Thus, the optical properties of both types of QDs are significantly influenced by the Se atoms.

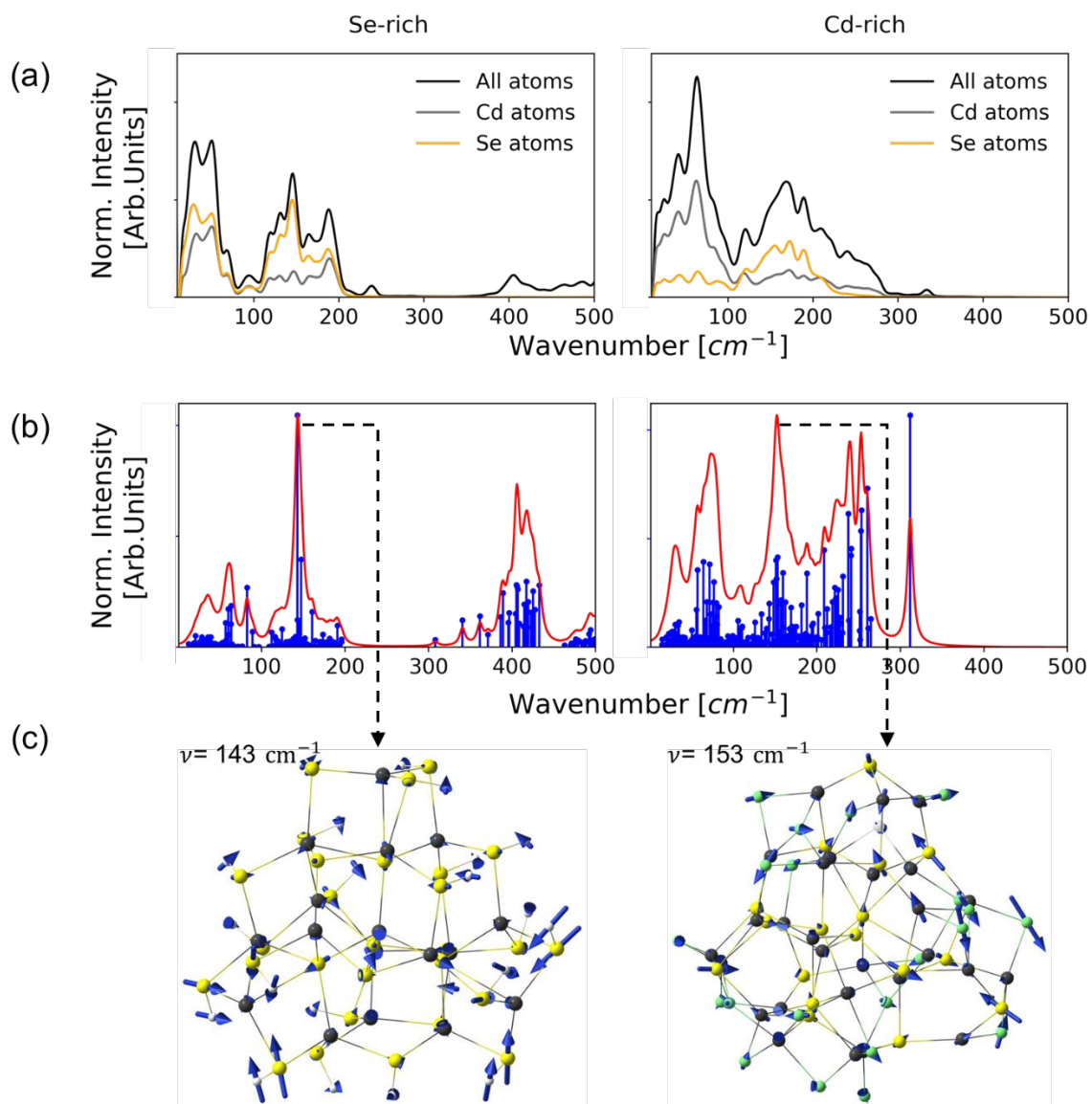


Figure 2. Vibrational properties of Se-rich and Cd-rich QDs. (a) The total and partial vibrational power spectra were obtained from the last 10ps of AIMD trajectories at 300K. (b) The Raman spectra were obtained from the optimized ground-state structure of QDs that are most stable among their types (that is Cd-rich and Se-rich). The spectra (shown in red) are obtained with Gaussian broadening (half-wide at half-height of 4 cm^{-1}) of the line-stick spectra (shown in blue) defining the positions of the vibrational normal modes and their Raman intensities. (c) The representative vibrational modes corresponding to the peaks in the Raman spectra (guided by the black dashed arrows) for Se-rich (143 cm^{-1}) and Cd-rich (153 cm^{-1}) QDs. The blue arrows reflect the displacement vectors of respective atoms. Atoms in yellow: Se, grey: Cd, white: H, green: Cl.

We also calculate the off-resonant Raman spectra (**Figure 2b**) of Se-rich and Cd-rich QDs to relate vibrational normal modes appearing in vibronic spectra and atomic motions visible in the power spectra. Although the Raman spectra are derived from static ground-state structures and the power spectra are derived from dynamic structures, some features of both spectra can be compared qualitatively. Markedly, for Se-rich and Cd-rich QDs, we find a good agreement between the peaks of power spectra and Raman spectra in the optical frequency region, which lie in the range of $\sim 140\text{-}160\text{ cm}^{-1}$. The normal modes corresponding to the Raman peaks for Se-rich (143 cm^{-1}) and Cd-rich (153 cm^{-1}) QDs are visualized in **Figure 2c**, where atomic displacements are represented with arrows for each atom and full visualization of these modes is provided in the Supplemental Material's animations. We note that for both QDs, movements of Se atoms have larger amplitudes when compared to that of Cd atoms. This agrees well with the findings from the decomposed power spectra in **Figure 2a**. Additionally, the movements of these Se atoms are out-of-phase, resembling the breathing of QD and confirming the nature of optical frequency modes dominated by bond-stretching motions. Both, the power and Raman spectra provide evidence for the larger contribution of Se atoms towards the optical phonon modes in Se-rich and Cd-rich QDs. Note that, the high-frequency Raman peaks for Se-rich QD above 300 cm^{-1} are assigned to the Se-H bending modes (Supplemental **Figure S3**). In contrast, the Cd-Cl stretching modes contribute mostly to the peaks above 220 cm^{-1} for Cd-rich QD (Supplemental **Figure S4**). Thus, the surface atoms of both QDs actively participate in the high-energy vibrational motions.

The simulated vibrational spectra of these CdSe QDs are different compared to that of CdSe nanocrystals.⁴⁷⁻⁴⁹ These apparent dissimilarities appear due to the large surface-to-volume ratio in these QDs. Beecher et al. point out that the overall characteristics of off-resonant Raman spectra predominantly depend on the size of cation-rich nonstoichiometric QDs.⁵⁰ From micro-Raman spectroscopy at room temperature, the study demonstrates that the smaller the QDs, the much

broader the Raman spectra in the range $>100\text{ cm}^{-1}$. The study also finds a broad Raman spectrum peak at $150\text{-}225\text{ cm}^{-1}$ for CdSe QD with a 2.1 nm diameter. As the simulated QDs in the present study are $\sim 1.5\text{ nm}$ in size, the Raman spectra in Figure 2a are broadened and shifted to a lower frequency for optical phonon modes. Moreover, we simulate off-resonant Raman spectra whereas many of the experiments report the corresponding resonant signals (which simulations involve much larger numerical cost and has limitation in terms of computational implementation).^{47,51,52} The off-resonant and resonant spectra may have very different peak intensities. Thus, the simulated spectrum for Cd-rich QD is only in qualitative agreement with its experimental counterpart.⁵⁰ Fundamentally, the largely different chemical environment of the surface atoms causes variability in Cd-Se bond stretching frequency and broadens the spectrum in the mentioned frequency range.

Electronic and Optical Properties

Atomic movements result in a dynamic electronic structure, including electronic bands, which, in turn, influence QD optical properties. **Figure 3a** presents the energy fluctuations (in the form of standard deviations) of the highest occupied molecular orbital (HOMO) and the lowest unoccupied molecular orbital (LUMO) of Se-rich and Cd-rich QDs. The HOMO and LUMO energies were determined in the structures extracted every 20 fs of the last 10ps of AIMD simulation (at 300K, a total of 500 structures).

The HOMO fluctuates more than LUMO in both Se-rich and Cd-rich QDs. This is consistent with the results derived from the vibrational analysis, where Se atomic motions contribute mainly to the optical vibrational modes. It also has been shown previously that the major contribution to the HOMO is from Se atoms.³² Therefore, the connection between the Se atom displacements to the optical phonon modes and greater fluctuation of HOMO, irrespective of the QD type, becomes more evident. Other than the vibrational motions of Se atoms in the optical frequency region, the higher mobility of surface atoms, as discussed earlier, also affects the band fluctuations. Since Se atoms are present in the core of the Cd-rich QD, the HOMO fluctuations are lower compared to those in Se-rich QD. On the other hand, the LUMO fluctuations are higher in Cd-rich QD compared to Se-rich QD because of the higher mobility of Cd surface atoms and also because of the higher contribution of Cd atoms to the LUMO.³² The synergistic effects of both surface mobility and high-frequency modes determine the overall fluctuations of the HOMO-LUMO gap. The results show that the fluctuations of the gap in Cd-rich QDs are smaller than that in Se-rich

QDs because of the higher fluctuation of Se surface atoms, which also contribute to the optical phonon modes. Fewer fluctuations indicate a stable HOMO-LUMO gap and therefore more consistent absorption and emission spectra. The Kohn-Sham orbitals representing HOMO and LUMO of the QDs at the end of the AIMD simulations are shown in **Figure 3b**. These orbitals look similar to the natural transition orbitals (NTOs) obtained in our previous work,³² where we imaged the transition of an electron during excitation from a low to a high energy state. In the previous report, we found that the delocalization of holes in Cd-rich QD was higher than that in Se-rich ones. A similar observation can be made here, where the HOMO of Cd-rich QDs appears more delocalized than that of Se-rich ones. This indicates that consistency is maintained in the electronic structure of Se-rich QD during thermal equilibration.

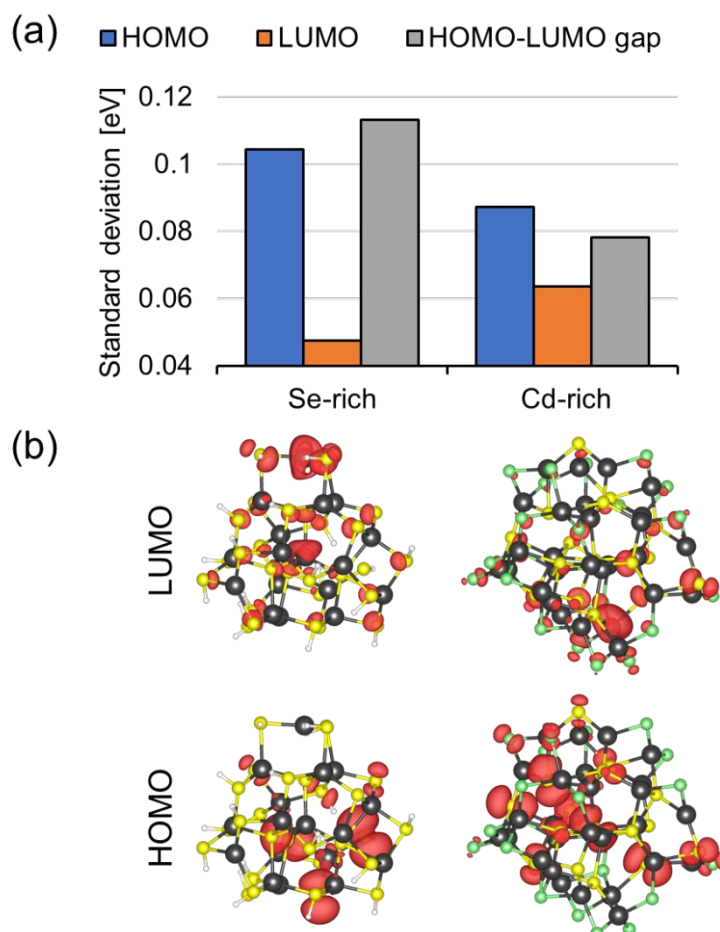


Figure 3. (a) The standard deviations of HOMO, LUMO, and HOMO-LUMO gap in Se-rich and Cd-rich QDs during the last 10 ps of AIMD trajectories at 300 K. (b) The Kohn-Sham orbitals showing the HOMO and LUMO of the Se-rich (left) and Cd-rich (right) QDs at the end of AIMD

simulation. The isosurface values of $0.0012 \text{ e } \text{\AA}^{-3}$ are used to generate the red isosurfaces for the Kohn-Sham orbitals. Atoms in yellow: Se, grey: Cd, white: H, green: Cl.

As mentioned earlier, the dynamics of six QD configurations of each type were analyzed for each QD type for 35 ps at 300 K. The HOMO and LUMO energy fluctuations of all six QDs for the last 10 ps of the simulation are shown in **Figure 4**. In contrast to HOMOs, the LUMOs for all six QDs of both QD types have similar energies. The Se-rich QDs have a range of HOMO-LUMO gaps because of the range of HOMO energies, while Cd-rich ones have more uniform HOMO-LUMO separation across several QD configurations. These results signify that an ensemble of atomically identical Se-rich QDs at ambient conditions would have a non-uniform HOMO-LUMO gap and therefore broadened absorption/emission spectra, whereas a similar ensemble of Cd-rich QDs would have a well-defined HOMO-LUMO gap and sharper absorption/emission spectra. Uniform emission from an ensemble of QDs would potentially result in intense high-quality luminescence. This is consistent with previous experimental results where Cd-rich QDs have higher photoluminescence stability and quantum yield.^{53,54}

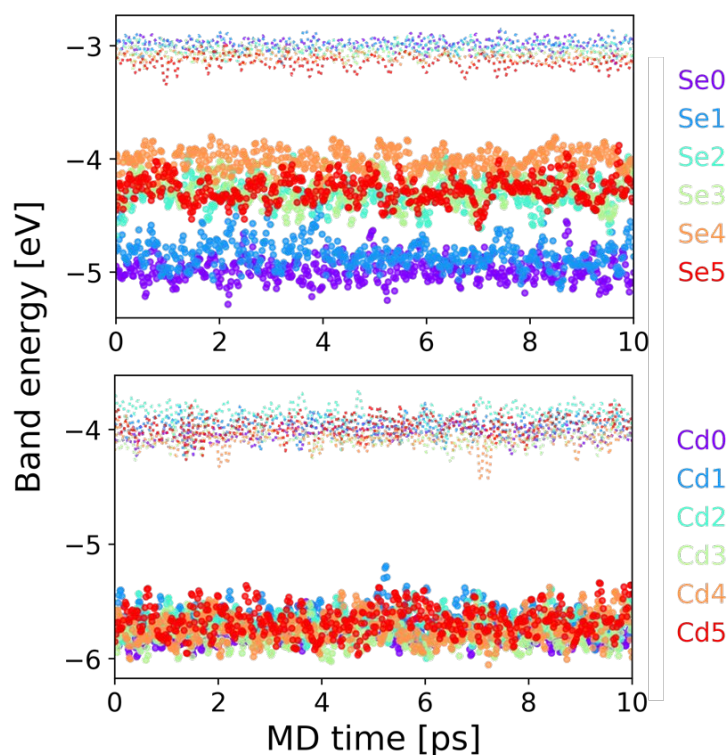


Figure 4. The fluctuations in HOMO and LUMO energies of six Se-rich (top) and six Cd-rich (bottom) QDs during the last 10 ps of AIMD trajectories at 300 K. The QDs are indexed from 0 to 5, in the order of increasing their ground state energy. The bigger dots (lower in energy) represent

the HOMO energy and the smaller dots (higher in energy) represent LUMO energy. These HOMO and LUMO energies are calculated every 20 fs throughout the simulation.

Noteworthy, in the previous investigation of QDs under static conditions, we found that several Se-rich and Cd-rich QD configurations have dark low-energy transitions in their absorption spectra. The current work (**Figure 4**) shows that all the Cd-rich configurations give rise to similar HOMO-LUMO energies, whereas Se-rich configurations have a range of HOMO-LUMO energies. This suggests that the low-energy transitions in Se-rich QDs would be long-lived, even after 35 ps of AIMD simulation, whereas those in Cd-rich QDs would heal with thermal equilibration. This conclusion is reasonable because both the effects of surface Se atom mobility and Se-dependent optical region vibrations work in tandem to affect the electronic properties of Se-rich QDs. The non-uniformity in electronic structures in Se-rich QDs would be reflected in the non-uniformity in their optical properties, making them poor candidates for single-photon emission applications.

Finally, we employ NAMD simulations to investigate the dynamics of charge carrier recombination in non-stoichiometric QDs and understand how the first excited state S_1 (HOMO \rightarrow LUMO) relaxes non-radiatively across the gap. NAMD simulations have proved beneficial in understanding the relaxation of excited states across a range of electronically active materials.^{19,24,55,56} **Figure 5a** shows electron-hole recombination as the population of excited electron decreases in Se-rich (Se0) and Cd-rich (Cd0) QDs - both of which have the lowest ground state energies and the widest HOMO-LUMO gap among their respective QD types as shown in **Figure 4**. The recombination is much faster in Cd-rich QD compared to Se-rich one. By assuming that the charge-carrier recombination timescale is described by a single-exponent process, the recombination time (τ) is calculated by fitting $f(t) = \exp(-t/\tau)$ to the decreasing carrier population. We find that the non-radiative recombination in Cd-rich QD investigated here is an order of magnitude faster than in Se-rich QD (16.6 ns vs 239.9 ns). The recombination rates are influenced by several factors, including the bandgap and its fluctuations, dephasing time, electron-phonon interaction-induced nonadiabatic couplings (NACs), etc. Usually, larger fluctuations of the HOMO-LUMO gap would result in a faster non-radiative relaxation. This trend, however, is not observed for the QDs studied here: HOMO-LUMO fluctuations (**Figure 3a**) are greater in Se-rich QD, but the electron-hole pair recombination is faster in Cd-rich QD. The recombination rates across the bandgap are also influenced by an average value of the bandgap, where the rate is

inversely related to the gap.⁵⁷ The Se0 QD has a larger average HOMO-LUMO gap (2.0 eV) compared to Cd0 (1.74 eV) and, therefore, this factor may be responsible for slower recombination of the electron-hole pair.

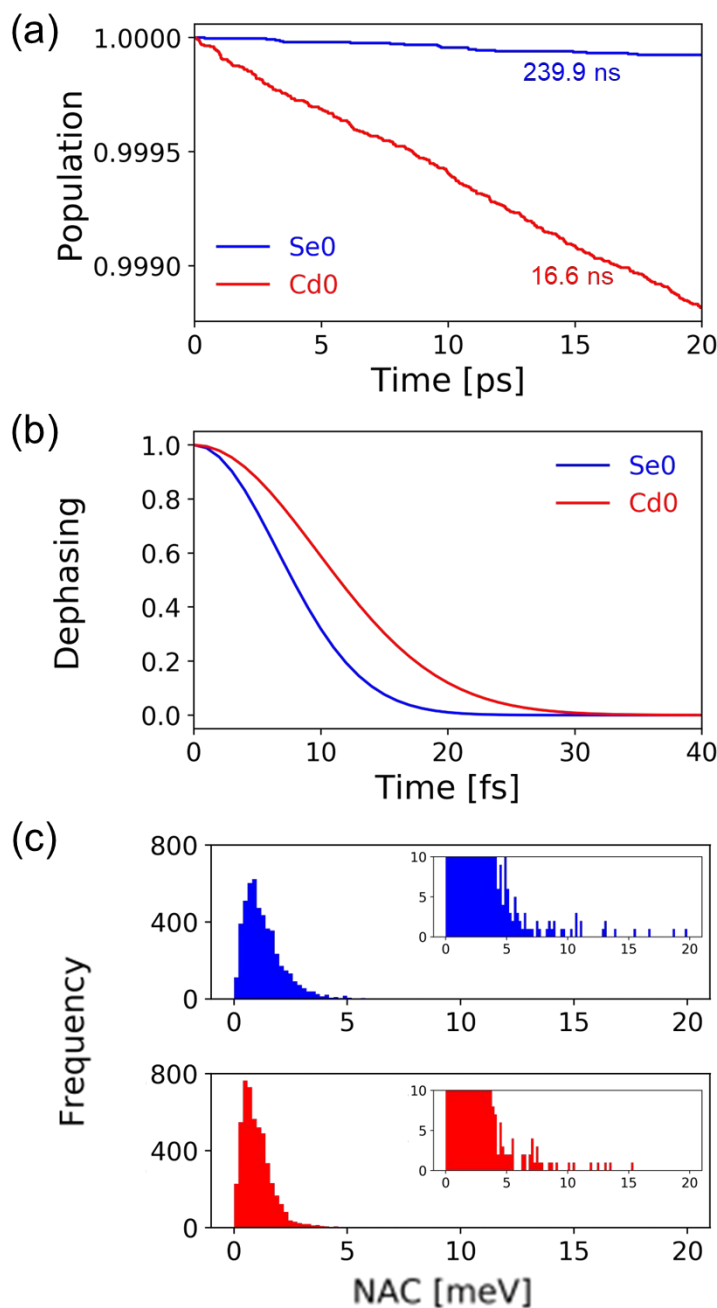


Figure 5. Non-adiabatic dynamics of QDs: (a) Charge carrier recombination rates determined from the decrease in the population of the first excited state, S_1 corresponding to HOMO→LUMO transition. The electron-hole pair recombination times were calculated by fitting depopulation curves to an exponential function, $f(t) = \exp(-t/\tau)$ and are shown alongside the curves. (b)

Pure-dephasing functions from HOMO-LUMO transition in Cd0 and Se0 QDs as a function of time. The decoherence occurs due to elastic electron-phonon scattering, partially suppressing the transition probability. (c) The histogram distribution of non-adiabatic coupling (NAC) values in Se-rich (top) and Cd-rich (bottom) QDs determined during the AIMD simulation. The insets contain a zoomed-in view of the respective histograms in the frequency range of (0,10). The Se-rich QD has higher frequencies for the higher NAC values.

Another key factor is the decoherence process that arises due to the elastic electron-phonon scattering, which strongly influences the quantum transitions.^{58,59} During electronic transitions in photoexcited systems, the ground, and excited states superpose transiently. However, elastic electron-phonons scattering causes this superposition to dephase, making the involved states in transition uncorrelated and evolving independently over time. We calculate the associated decoherence time as the pure-dephasing time that has been formulated using optical response theory and applied to various types of materials.⁶⁰ The plotted cumulant dephasing functions in **Figure 5b** suggests that the dephasing in these QDs occurs in ultrafast timescale, within a few tenths of femtosecond (fs). We calculate the dephasing time (τ') by fitting a Gaussian function ($f(t) = \exp[-(t/\tau')^2/2]$). The estimated dephasing time for Se0 (6.6 fs) is 1.5 times faster than in Cd0 (9.7 fs). The evaluated trend of dephasing time primarily arises from the extent of energy fluctuations of associated energy states (HOMO and LUMO here) over time, which is higher in Se-rich QDs. Additionally, the faster the decoherence, the slower the quantum dynamics as we find in the quantum-Zeno effect.⁶¹ Thus, the faster quantum decoherence significantly reduces the chance of electron relaxation through transient superposition of HOMO-LUMO wavefunctions in Se-rich QD. Furthermore, we inspected the NACs between HOMO and LUMO during the MD simulation to determine their effect on the electron-hole pair recombination (**Figure 5c**). The interaction between electronic states and vibrational motion of atomic sites (frequently denoted as an electron-vibrational or electron-phonon coupling in finite systems or solid materials, respectively) can be calculated or quantified experimentally in terms of Hyang-Rhys factors.⁶² These interactions facilitate carrier non-radiative dynamics and give rise to NACs. Typically, NACs are straightforward to calculate, while these quantities are challenging to measure experimentally. The NACs for Se0 have broader distribution compared to that of Cd0, with higher NAC values being more frequent in Se0. Subsequently, the average NAC in Se0 (1.38 meV) is higher than that in Cd0 (1.06 meV), reflecting higher effective electron-phonon coupling in Se-rich QDs. The overall stronger electron-phonon interactions in Se-rich QD also support our finding that the dephasing process in these QDs is faster in time. Hence, among several factors, the

magnitude of the energy gap and quantum decoherence are most likely the dominant factors that control the non-radiative recombination processes in non-stoichiometric QDs. Observed complex relationships between surface passivation, excited-state dynamics, and structural fluctuations in non-stoichiometric QDs warrant future modeling studies. Additionally, the presence of point-defects in the QDs can substantially impact the carrier relaxation process by introducing in-gap states that may act as non-radiative recombination centers for separated electron-hole pairs. However, the current study does not include such effects and focuses on the impact of electron-vibrational coupling on the charge relaxation. Our future efforts will focus considering other factors, such as solvent effect, surface point defects, and imperfect surface passivation (due to ligand loss) to understand the charge relaxation in QDs to a greater extent. Note that, severely limited experimental observations restrict us from validating our computational findings with those in details. However, with the advancements in experimental synthesis procedures and characterizations tools we strongly believe that nonstoichiometric small QDs will be studied in near future.

In summary, this computational work reports a detailed investigation of the influence of thermally induced structural and vibrational fluctuations on the optoelectronic properties of non-stoichiometric CdSe QD clusters at ambient conditions. Due to the undercoordinated environment of atoms on the surface, we find that Se atoms are more dynamic in Se-rich QDs, and Cd atoms are so in Cd-rich ones. The vibrational analysis reveals that irrespective of the QD type, Se atoms always have a higher contribution towards high-frequency vibrations (prototypical optical phonons related to the bond stretching), suggesting a higher influence on the HOMO energies of QDs. The electronic structures are dependent on the surface fluctuations, and they are affected by high-frequency vibrations. Overall, we determine that the HOMO-LUMO gap of Se-rich QDs fluctuates more compared to that of Cd-rich systems. In Se-rich QDs, the surface Se atoms are more dynamic and vibrate more in the optical phonon region, whereas in Cd-rich ones, Se atoms are well passivated and sterically constrained, which results in less thermal and optical fluctuations. Furthermore, the Se-rich QDs with various configurations of ligands on the surface show a range of HOMO-LUMO gaps, reflecting the presence of multiple long-lived low-energy transitions. In contrast, the set of analogous Cd-rich QDs reveals a near-constant HOMO-LUMO gap, pointing to the stable emission and faster thermal healing of their electronic structures. Interestingly, the non-adiabatic transition rates for LUMO \rightarrow HOMO demonstrate faster non-radiative

recombination of Cd-rich QDs compared to Se-rich QDs. The faster decoherence processes and larger time-averaged bandgap in Se-rich QD are the primary reasons behind this trend. Altogether, the atomistic investigation carried on in this study provides insights into the differences in the optical and electronic properties of anion-rich and cation-rich QDs at ambient conditions. These results help to rationalize previous experimental studies showing superior photoluminescence of cation-rich QDs compared to anion-rich QDs.

Acknowledgments

The work at Los Alamos National Laboratory (LANL) was supported by the Laboratory Directed Research and Development (LDRD) program at LANL under project 20200213DR. This work was done in part at the Center for Nonlinear Studies (CNLS) and the Center for Integrated Nanotechnologies (CINT), a U.S. Department of Energy and Office of Basic Energy Sciences user facility, at LANL. This research used resources provided by the LANL Institutional Computing Program. Los Alamos National Laboratory is operated by Triad National Security, LLC, for the National Nuclear Security Administration of the U.S. Department of Energy (Contract No. 89233218NCA000001). All authors thank Dr. Victor I. Klimov for fruitful discussions. DG acknowledges the IIT Delhi SEED Grant (PLN12/04MS) and the IIT Delhi HPC facility for computational resources.

References

- (1) Yoffe, A. D. Low-Dimensional Systems: Quantum Size Effects and Electronic Properties of Semiconductor Microcrystallites (Zero-Dimensional Systems) and Some Quasi-Two-Dimensional Systems. *Advances in Physics* **1993**, *42* (2), 173–262. <https://doi.org/10.1080/00018739300101484>.
- (2) Yoffe, A. D. Semiconductor Quantum Dots and Related Systems: Electronic, Optical, Luminescence and Related Properties of Low Dimensional Systems. *Advances in Physics* **2001**, *50* (1), 1–208. <https://doi.org/10.1080/00018730010006608>.
- (3) Liu, L.; Peng, Q.; Li, Y. Preparation of CdSe Quantum Dots with Full Color Emission Based on a Room Temperature Injection Technique. *Inorg. Chem.* **2008**, *47* (11), 5022–5028. <https://doi.org/10.1021/ic800368u>.

- (4) Arquer, F. P. G. de; Talapin, D. V.; Klimov, V. I.; Arakawa, Y.; Bayer, M.; Sargent, E. H. Semiconductor Quantum Dots: Technological Progress and Future Challenges. *Science* **2021**, *373* (6555). <https://doi.org/10.1126/science.aaz8541>.
- (5) Pietryga, J. M.; Park, Y.-S.; Lim, J.; Fidler, A. F.; Bae, W. K.; Brovelli, S.; Klimov, V. I. Spectroscopic and Device Aspects of Nanocrystal Quantum Dots. *Chem. Rev.* **2016**, *116* (18), 10513–10622. <https://doi.org/10.1021/acs.chemrev.6b00169>.
- (6) Cotta, M. A. Quantum Dots and Their Applications: What Lies Ahead? *ACS Appl. Nano Mater.* **2020**, *3* (6), 4920–4924. <https://doi.org/10.1021/acsanm.0c01386>.
- (7) Colvin, V. L.; Schlamp, M. C.; Alivisatos, A. P. Light-Emitting Diodes Made from Cadmium Selenide Nanocrystals and a Semiconducting Polymer. *Nature* **1994**, *370* (6488), 354–357. <https://doi.org/10.1038/370354a0>.
- (8) Pan, Z.; Rao, H.; Mora-Seró, I.; Bisquert, J.; Zhong, X. Quantum Dot-Sensitized Solar Cells. *Chem. Soc. Rev.* **2018**, *47* (20), 7659–7702. <https://doi.org/10.1039/C8CS00431E>.
- (9) Mallick, S.; Kumar, P.; Koner, A. L. Freeze-Resistant Cadmium-Free Quantum Dots for Live-Cell Imaging. *ACS Appl. Nano Mater.* **2019**, *2* (2), 661–666. <https://doi.org/10.1021/acsanm.8b02231>.
- (10) Zhou, Y.; Yang, S.; Fan, D.; Reilly, J.; Zhang, H.; Yao, W.; Huang, J. Carbon Quantum Dot/TiO₂ Nanohybrids: Efficient Photocatalysts for Hydrogen Generation via Intimate Contact and Efficient Charge Separation. *ACS Appl. Nano Mater.* **2019**, *2* (2), 1027–1032. <https://doi.org/10.1021/acsanm.8b02310>.
- (11) Lv, Z.; Wang, Y.; Chen, J.; Wang, J.; Zhou, Y.; Han, S.-T. Semiconductor Quantum Dots for Memories and Neuromorphic Computing Systems. *Chem. Rev.* **2020**, *120* (9), 3941–4006. <https://doi.org/10.1021/acs.chemrev.9b00730>.
- (12) Pu, Y.; Cai, F.; Wang, D.; Wang, J.-X.; Chen, J.-F. Colloidal Synthesis of Semiconductor Quantum Dots toward Large-Scale Production: A Review. *Ind. Eng. Chem. Res.* **2018**, *57* (6), 1790–1802. <https://doi.org/10.1021/acs.iecr.7b04836>.

- (13) Fan, X.-B.; Yu, S.; Zhan, F.; Li, Z.-J.; Gao, Y.-J.; Li, X.-B.; Zhang, L.-P.; Tao, Y.; Tung, C.-H.; Wu, L.-Z. Nonstoichiometric $\text{Cu}_x\text{In}_y\text{S}$ Quantum Dots for Efficient Photocatalytic Hydrogen Evolution. *ChemSusChem* **2017**, *10* (24), 4833–4838. <https://doi.org/10.1002/cssc.201701950>.
- (14) Huang, M.-Y.; Li, X.-B.; Gao, Y.-J.; Li, J.; Wu, H.-L.; Zhang, L.-P.; Tung, C.-H.; Wu, L.-Z. Surface Stoichiometry Manipulation Enhances Solar Hydrogen Evolution of CdSe Quantum Dots. *J. Mater. Chem. A* **2018**, *6* (14), 6015–6021. <https://doi.org/10.1039/C8TA00385H>.
- (15) Xia, W.; Wu, J.; Hu, J.-C.; Sun, S.; Li, M.-D.; Liu, H.; Lan, M.; Wang, F. Highly Efficient Photocatalytic Conversion of CO_2 to CO Catalyzed by Surface-Ligand-Removed and Cd-Rich CdSe Quantum Dots. *ChemSusChem* **2019**, *12* (20), 4617–4622. <https://doi.org/10.1002/cssc.201901633>.
- (16) Kilina, S. V.; Tamukong, P. K.; Kilin, D. S. Surface Chemistry of Semiconducting Quantum Dots: Theoretical Perspectives. *Acc. Chem. Res.* **2016**, *49* (10), 2127–2135. <https://doi.org/10.1021/acs.accounts.6b00196>.
- (17) Troparevsky, M. C.; Kronik, L.; Chelikowsky, J. R. Optical Properties of CdSe Quantum Dots. *J. Chem. Phys.* **2003**, *119* (4), 2284–2287. <https://doi.org/10.1063/1.1585013>.
- (18) Puzder, A.; Williamson, A. J.; Gygi, F.; Galli, G. Self-Healing of CdSe Nanocrystals: First-Principles Calculations. *Phys. Rev. Lett.* **2004**, *92* (21), 217401. <https://doi.org/10.1103/PhysRevLett.92.217401>.
- (19) Kilina, S.; Kilin, D.; Tretiak, S. Light-Driven and Phonon-Assisted Dynamics in Organic and Semiconductor Nanostructures. *Chem. Rev.* **2015**, *115* (12), 5929–5978. <https://doi.org/10.1021/acs.chemrev.5b00012>.
- (20) Hong, Y.; Wu, Y.; Wu, S.; Wang, X.; Zhang, J. Overview of Computational Simulations in Quantum Dots. *Israel Journal of Chemistry* **2019**, *59* (8), 661–672. <https://doi.org/10.1002/ijch.201900026>.

- (21) Giansante, C.; Infante, I. Surface Traps in Colloidal Quantum Dots: A Combined Experimental and Theoretical Perspective. *J. Phys. Chem. Lett.* **2017**, *8* (20), 5209–5215. <https://doi.org/10.1021/acs.jpcclett.7b02193>.
- (22) Houtepen, A. J.; Hens, Z.; Owen, J. S.; Infante, I. On the Origin of Surface Traps in Colloidal II–VI Semiconductor Nanocrystals. *Chem. Mater.* **2017**, *29* (2), 752–761. <https://doi.org/10.1021/acs.chemmater.6b04648>.
- (23) Kilina, S.; Ivanov, S.; Tretiak, S. Effect of Surface Ligands on Optical and Electronic Spectra of Semiconductor Nanoclusters. *J. Am. Chem. Soc.* **2009**, *131* (22), 7717–7726. <https://doi.org/10.1021/ja9005749>.
- (24) Kilina, S.; Velizhanin, K. A.; Ivanov, S.; Prezhdo, O. V.; Tretiak, S. Surface Ligands Increase Photoexcitation Relaxation Rates in CdSe Quantum Dots. *ACS Nano* **2012**, *6* (7), 6515–6524. <https://doi.org/10.1021/nn302371q>.
- (25) Liu, J.; Kilina, S. V.; Tretiak, S.; Prezhdo, O. V. Ligands Slow Down Pure-Dephasing in Semiconductor Quantum Dots. *ACS Nano* **2015**, *9* (9), 9106–9116. <https://doi.org/10.1021/acs.nano.5b03255>.
- (26) Fischer, S. A.; Crotty, A. M.; Kilina, S. V.; Ivanov, S. A.; Tretiak, S. Passivating Ligand and Solvent Contributions to the Electronic Properties of Semiconductor Nanocrystals. *Nanoscale* **2012**, *4* (3), 904–914. <https://doi.org/10.1039/C2NR11398H>.
- (27) Tamukong, P. K.; Peiris, W. D. N.; Kilina, S. Computational Insights into CdSe Quantum Dots' Interactions with Acetate Ligands. *Phys. Chem. Chem. Phys.* **2016**, *18* (30), 20499–20510. <https://doi.org/10.1039/C6CP01665K>.
- (28) Azpiroz, J. M.; Matxain, J. M.; Infante, I.; Lopez, X.; Ugalde, J. M. A DFT/TDDFT Study on the Optoelectronic Properties of the Amine-Capped Magic (CdSe)₁₃ Nanocluster. *Phys. Chem. Chem. Phys.* **2013**, *15* (26), 10996–11005. <https://doi.org/10.1039/C3CP51687C>.
- (29) Albert, V. V.; Ivanov, S. A.; Tretiak, S.; Kilina, S. V. Electronic Structure of Ligated CdSe Clusters: Dependence on DFT Methodology. *J. Phys. Chem. C* **2011**, *115* (32), 15793–15800. <https://doi.org/10.1021/jp202510z>.

- (30) Kelley, A. M. Exciton-Optical Phonon Coupling in II-VI Semiconductor Nanocrystals. *J. Chem. Phys.* **2019**, *151* (14), 140901. <https://doi.org/10.1063/1.5125147>.
- (31) Weiss, E. A. Organic Molecules as Tools To Control the Growth, Surface Structure, and Redox Activity of Colloidal Quantum Dots. *Acc. Chem. Res.* **2013**, *46* (11), 2607–2615. <https://doi.org/10.1021/ar400078u>.
- (32) Bhati, M.; Ivanov, S. A.; Senftle, T. P.; Tretiak, S.; Ghosh, D. Nature of Electronic Excitations in Small Non-Stoichiometric Quantum Dots. *J. Mater. Chem. A* **2022**, *10* (10), 5212–5220. <https://doi.org/10.1039/D1TA07983B>.
- (33) Ghosh, D.; Ivanov, S. A.; Tretiak, S. Structural Dynamics and Electronic Properties of Semiconductor Quantum Dots: Computational Insights. *Chem. Mater.* **2021**, *33* (19), 7848–7857. <https://doi.org/10.1021/acs.chemmater.1c02514>.
- (34) de Mello Donegá, C.; Bode, M.; Meijerink, A. Size- and Temperature-Dependence of Exciton Lifetimes in CdSe Quantum Dots. *Phys. Rev. B* **2006**, *74* (8), 085320. <https://doi.org/10.1103/PhysRevB.74.085320>.
- (35) Balan, A. D.; Eshet, H.; Olshansky, J. H.; Lee, Y. V.; Rabani, E.; Alivisatos, A. P. Effect of Thermal Fluctuations on the Radiative Rate in Core/Shell Quantum Dots. *Nano Lett.* **2017**, *17* (3), 1629–1636. <https://doi.org/10.1021/acs.nanolett.6b04816>.
- (36) Saniepay, M.; Mi, C.; Liu, Z.; Abel, E. P.; Beaulac, R. Insights into the Structural Complexity of Colloidal CdSe Nanocrystal Surfaces: Correlating the Efficiency of Nonradiative Excited-State Processes to Specific Defects. *J. Am. Chem. Soc.* **2018**, *140* (5), 1725–1736. <https://doi.org/10.1021/jacs.7b10649>.
- (37) Kobayashi, Y.; Nishimura, T.; Yamaguchi, H.; Tamai, N. Effect of Surface Defects on Auger Recombination in Colloidal CdS Quantum Dots. *J. Phys. Chem. Lett.* **2011**, *2* (9), 1051–1055. <https://doi.org/10.1021/jz200254n>.
- (38) Grimaldi, G.; Geuchies, J. J.; van der Stam, W.; du Fossé, I.; Brynjarsson, B.; Kirkwood, N.; Kinge, S.; Siebbeles, L. D. A.; Houtepen, A. J. Spectroscopic Evidence for the Contribution of

Holes to the Bleach of Cd-Chalcogenide Quantum Dots. *Nano Lett.* **2019**, *19* (5), 3002–3010. <https://doi.org/10.1021/acs.nanolett.9b00164>.

(39) du Fossé, I.; ten Brinck, S.; Infante, I.; Houtepen, A. J. Role of Surface Reduction in the Formation of Traps in N-Doped II–VI Semiconductor Nanocrystals: How to Charge without Reducing the Surface. *Chem. Mater.* **2019**, *31* (12), 4575–4583. <https://doi.org/10.1021/acs.chemmater.9b01395>.

(40) Aharonovich, I.; Englund, D.; Toth, M. Solid-State Single-Photon Emitters. *Nature Photon* **2016**, *10* (10), 631–641. <https://doi.org/10.1038/nphoton.2016.186>.

(41) Soloviev, V. N.; Eichhöfer, A.; Fenske, D.; Banin, U. Molecular Limit of a Bulk Semiconductor: Size Dependence of the “Band Gap” in CdSe Cluster Molecules. *J. Am. Chem. Soc.* **2000**, *122* (11), 2673–2674. <https://doi.org/10.1021/ja9940367>.

(42) Soloviev, V. N.; Eichhöfer, A.; Fenske, D.; Banin, U. Size-Dependent Optical Spectroscopy of a Homologous Series of CdSe Cluster Molecules. *J. Am. Chem. Soc.* **2001**, *123* (10), 2354–2364. <https://doi.org/10.1021/ja003598j>.

(43) Dmitruk, I.; Belosludov, R. V.; Dmytruk, A.; Noda, Y.; Barnakov, Y.; Park, Y.-S.; Kasuya, A. Experimental and Computational Studies of the Structure of CdSe Magic-Size Clusters. *J. Phys. Chem. A* **2020**, *124* (17), 3398–3406. <https://doi.org/10.1021/acs.jpca.0c00782>.

(44) Schmitt-Rink, S.; Miller, D. A. B.; Chemla, D. S. Theory of the Linear and Nonlinear Optical Properties of Semiconductor Microcrystallites. *Phys. Rev. B* **1987**, *35* (15), 8113–8125. <https://doi.org/10.1103/PhysRevB.35.8113>.

(45) Klein, M. C.; Hache, F.; Ricard, D.; Flytzanis, C. Size Dependence of Electron-Phonon Coupling in Semiconductor Nanospheres: The Case of CdSe. *Phys. Rev. B* **1990**, *42* (17), 11123–11132. <https://doi.org/10.1103/PhysRevB.42.11123>.

(46) Kelley, A. M. Electron–Phonon Coupling in CdSe Nanocrystals from an Atomistic Phonon Model. *ACS Nano* **2011**, *5* (6), 5254–5262. <https://doi.org/10.1021/nn201475d>.

- (47) Lin, C.; Kelley, D. F.; Rico, M.; Kelley, A. M. The “Surface Optical” Phonon in CdSe Nanocrystals. *ACS Nano* **2014**, *8* (4), 3928–3938. <https://doi.org/10.1021/nn5008513>.
- (48) Cheng, Y. C.; Jin, C. Q.; Gao, F.; Wu, X. L.; Zhong, W.; Li, S. H.; Chu, P. K. Raman Scattering Study of Zinc Blende and Wurtzite ZnS. *Journal of Applied Physics* **2009**, *106* (12), 123505. <https://doi.org/10.1063/1.3270401>.
- (49) Shiang, J. J.; Risbud, S. H.; Alivisatos, A. P. Resonance Raman Studies of the Ground and Lowest Electronic Excited State in CdS Nanocrystals. *J. Chem. Phys.* **1993**, *98* (11), 8432–8442. <https://doi.org/10.1063/1.464501>.
- (50) Beecher, A. N.; Dziatko, R. A.; Steigerwald, M. L.; Owen, J. S.; Crowther, A. C. Transition from Molecular Vibrations to Phonons in Atomically Precise Cadmium Selenide Quantum Dots. *J. Am. Chem. Soc.* **2016**, *138* (51), 16754–16763. <https://doi.org/10.1021/jacs.6b10705>.
- (51) Grenland, J. J.; Lin, C.; Gong, K.; Kelley, D. F.; Kelley, A. M. Resonance Raman Investigation of the Interaction between Aromatic Dithiocarbamate Ligands and CdSe Quantum Dots. *J. Phys. Chem. C* **2017**, *121* (12), 7056–7061. <https://doi.org/10.1021/acs.jpcc.7b01651>.
- (52) Rolo, A. G.; Vasilevskiy, M. I. Raman Spectroscopy of Optical Phonons Confined in Semiconductor Quantum Dots and Nanocrystals. *Journal of Raman Spectroscopy* **2007**, *38* (6), 618–633. <https://doi.org/10.1002/jrs.1746>.
- (53) Jasieniak, J.; Mulvaney, P. From Cd-Rich to Se-Rich – the Manipulation of CdSe Nanocrystal Surface Stoichiometry. *J. Am. Chem. Soc.* **2007**, *129* (10), 2841–2848. <https://doi.org/10.1021/ja066205a>.
- (54) Wei, H. H.-Y.; Evans, C. M.; Swartz, B. D.; Neukirch, A. J.; Young, J.; Prezhdo, O. V.; Krauss, T. D. Colloidal Semiconductor Quantum Dots with Tunable Surface Composition. *Nano Lett.* **2012**, *12* (9), 4465–4471. <https://doi.org/10.1021/nl3012962>.
- (55) Ghosh, D.; Acharya, D.; Pedesseau, L.; Katan, C.; Even, J.; Tretiak, S.; Neukirch, A. J. Charge Carrier Dynamics in Two-Dimensional Hybrid Perovskites: Dion–Jacobson vs. Ruddlesden–Popper Phases. *J. Mater. Chem. A* **2020**, *8* (42), 22009–22022. <https://doi.org/10.1039/D0TA07205B>.

- (56) Wang, Y.; Pedesseau, L.; Katan, C.; Even, J.; Prezhdo, O. V.; Tretiak, S.; Ghosh, D.; Neukirch, A. J. Nonadiabatic Molecular Dynamics Analysis of Hybrid Dion–Jacobson 2D Leads Iodide Perovskites. *Appl. Phys. Lett.* **2021**, *119* (20), 201102. <https://doi.org/10.1063/5.0066087>.
- (57) Englman, R.; Jortner, J. The Energy Gap Law for Non-Radiative Decay in Large Molecules. *Journal of Luminescence* **1970**, *1–2*, 134–142. [https://doi.org/10.1016/0022-2313\(70\)90029-3](https://doi.org/10.1016/0022-2313(70)90029-3).
- (58) Prezhdo, O. V.; Rossky, P. J. Evaluation of Quantum Transition Rates from Quantum-Classical Molecular Dynamics Simulations. *J. Chem. Phys.* **1997**, *107* (15), 5863–5878. <https://doi.org/10.1063/1.474312>.
- (59) Zhang, Z.; Fang, W.-H.; Tokina, M. V.; Long, R.; Prezhdo, O. V. Rapid Decoherence Suppresses Charge Recombination in Multi-Layer 2D Halide Perovskites: Time-Domain Ab Initio Analysis. *Nano Lett.* **2018**, *18* (4), 2459–2466. <https://doi.org/10.1021/acs.nanolett.8b00035>.
- (60) Mukamel, S. *Principles of Nonlinear Optical Spectroscopy*; Oxford University Press on Demand, 1999.
- (61) Kilina, S. V.; Neukirch, A. J.; Habenicht, B. F.; Kilin, D. S.; Prezhdo, O. V. Quantum Zeno Effect Rationalizes the Phonon Bottleneck in Semiconductor Quantum Dots. *Phys. Rev. Lett.* **2013**, *110* (18), 180404. <https://doi.org/10.1103/PhysRevLett.110.180404>.
- (62) Kelley, A. M. Electron–Phonon Coupling in CdSe Nanocrystals. *J. Phys. Chem. Lett.* **2010**, *1* (9), 1296–1300. <https://doi.org/10.1021/jz100123b>.